ECN-C--05-050

TNO BOUNDARY LAYER TUNNEL

Quality of Velocity Profiles

M. Blaas, G. P. Corten, P. Schaak

MAY 2005

Preface

For ECN's experiments with scaled wind farms in the boundary-layer wind tunnel of TNO in Apeldoorn knowledge of the general characteristics of the wind tunnel flow are extremely important. This report summarizes the tunnel performance as far as can be determined after three entries carried out in May and November 2003 and September 2004. This document is an extension to the information in the internship report by Agnès Monseur (Monseur, 2004) and the internal TNO documentation on the wind tunnel flow (TNO, 1995).

Acknowledgement

This work was supported by the Programme Renewable Energy *(Programma Duurzame Energie*) in the Netherlands, which is carried out by the Netherlands Agency for Energy and Environment (*SenterNovem*) under the authority of the ministry of economic affairs *(Ministerie van Economische Zaken*). The work was carried out within the project Heat and Flux, Fundamental, project number 2020-03-11-10-007, order number 48000027.

Abstract

The velocity profiles and Reynolds stresses of the empty boundary layer tunnel of TNO Apeldoorn have been characterized. This tunnel has a measurement section of 3 m wide, 2 meters high, and 9 meters long. The tunnel was set up to represent an offshore atmospheric boundary layer scaled by a factor of 400. The measurements were carried out by a hotwire traverse system. The results are listed below.

characteristic	*neutrally stable, offshore atmosphere in reality*	*empty TNO-tunnel (6-9 m/s)*
vertical velocity profile	logarithmic	logarithmic up to 80 cm height (320m on scale) over first 9 m (3600m on scale); separate fits of lower 17 cm yield 25% larger values for u_*.
horizontal velocity profile	flat	varies by 3% over tunnel width between 17 and 37 cm height (68m - 148m on scale)
friction velocity u_*	constant	varies by 9% over first 9 meters
shear stress (Reynolds stress, $<u'w'>$)	'independent' of height	'independent' of height in first 4.5 meters. decreases about 30% in 80 cm height in next 4.5 meters.
surface roughness z_0	0.2 mm	$0.4\text{-}7.2*10^{-4}$ mm (0.02-0.3 mm on scale)
dynamic pressure gradient in wind direction dP/dx	'none'	≈ -0.5 Pa/m (-1.3 Pa/km on scale)

We conclude that the test section of the tunnel represents offshore conditions well in an on-scale area ranging from sea level to 320 m altitude and extending over 3.6 km in flow direction.

CONTENTS

1. INTRODUCTION

In 2003 and 2004 the ECN unit Wind Energy has undertaken three series of experiments in the boundary layer wind tunnel at TNO Apeldoorn. The principle goals are to study the performance and characteristics of single and especially multiple scale models of wind turbines in offshore wind farms under controlled circumstances (Corten, 2001; Corten and Schaak, 2003; Corten & Schaak, 2004; Corten, Lindenburg & Schaak, 2002). In order to judge the results of the wind-farm measurements, the tunnel flow conditions without turbines should be clear. This report characterizes the flow and Reynolds stress of the -so called- 'empty tunnel'.

At this moment three entries of about two weeks tunnel time each have been carried out which started in May and November 2003, and September 2004, respectively. During the entries not only direct pressure and velocity measurements were taken with an anemometer and a manometer, but also velocity data were taken with a hotwire probe. The hotwire probe is remotely movable during measurement sessions so that 'scans' can be to obtain spatial information of the air flow. During the first two entries hotwire scans were made of an 'empty tunnel', *i.e.,* a tunnel without obstacles other than the hotwire frame, anemometer, manometer, and a barrier in the front zone to set up the desired boundary layer profile. For the ECN experiments the boundary layer should be representative for offshore conditions (calm sea) on a scale of 1:400. The session names, dates and short description of the measurements are listed in Table 3.1.

In this report a summary of the horizontal and vertical structure of the flow generated in the empty tunnel is given for various tunnel speeds. We discuss the Reynolds-averaged vertical profiles of horizontal velocity as well as the profiles of the Reynolds stresses. Particular issues of concern are the quality and consistency of the profiles and their scaling with respect to the size of the wind farms used. The along-tunnel and across-tunnel variation of the flow will also be discussed.

The outline of this report is as follows. In the next section a brief description of the tunnel lay out and hot wire probe is given. The third section discusses the general quality of the data and the most important systematic deviations from the expected. Section 4 discusses the vertical and horizontal profiles of velocity and Reynolds stresses. Finally sections 5 gives general conclusions in terms of the quality of the scaled atmospheric boundary layer.

2. DESCRIPTION OF TUNNEL LAY OUT AND METHODS

2.1 Tunnel Lay Out

The TNO boundary layer wind tunnel is located at the site of TNO Apeldoorn, The Netherlands. The tunnel has been designed to simulate atmospheric boundary layers on scale 1:1 to 1:2500 and is capable of creating flows with a nominal speed ranging from 0.2 to 20 m/s. For ECN the appropriate scale is 1:400, such that the standard turbine hub height of 267 mm represents 106.8 m in reality and the rotor of 250 mm diameter represents a 100 m rotor. The nominal tunnel speeds for ECN's purposes vary from 6 to about 12 m/s.

The tunnel top view and side view are shown in figure 2.1. The air inlet is positioned at a right angle to the main channel. Inside the inlet heaters and filters are present. Steering fins to guide the flow to the right after entering the intake are not present however. This implies that any secondary circulation due to flow curvature is not interrupted. At the end of the inlet section an anti-turbulence gauze has been placed. After the inlet section the channel contracts to accelerate the flow. Beyond the contraction the channel is straight with a width of 3 m and a height of 2 m. The channel consists of an "up-stream" section of about 14 m length and the proper test section of 11.5 m length. The floor of the up-stream section may be covered with material of the appropriate roughness to generate a scaled neutral atmospheric boundary layer. For the ECN experiments marine (offshore) conditions are appropriate. In those cases no other objects are present than a single barrier of 185 mm high in the front of the run-up area. Please note that the tunnel has a left-handed coordinate system: the vector product of x and y points into negative z direction.

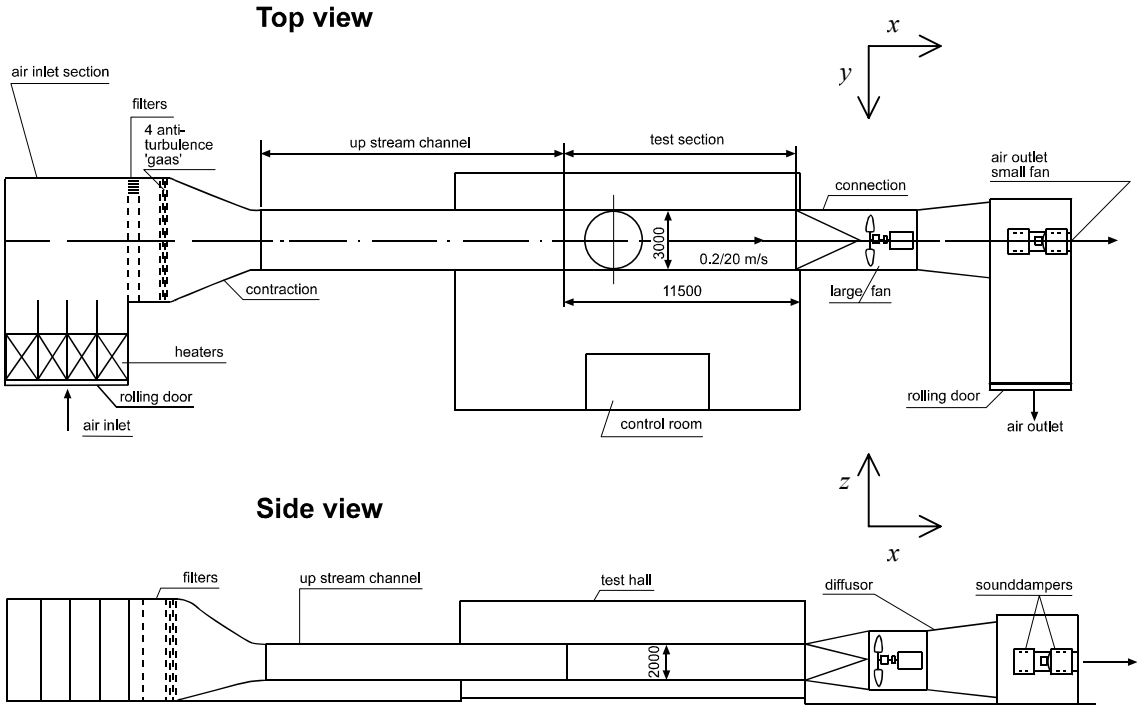

Figure 2.1 *Top and side view of TNO atmospheric boundary layer tunnel. Sizes in mm.*

2.2 Hotwire Measurement Method

The hotwire probes are mounted in a fork-shaped device, which is attached to a movable frame. This frame is in turn suspended to a movable beam spanning the width of the tunnel (see Figures 2.2 and 2.3). The total system is called the *hot wire traverse system*. Tests have shown that flow blockage near the tunnel ceiling by the traverse system causes considerable disturbance of the flow. Moving the hotwire from far downstream towards an anemometer at hub height in the center of the tunnel caused the anemometer readings to increase by about 3%. At this moment we do not have sufficient data to correct for this acceleration.

The hotwire data are converted by TNO to a representative velocity by use of the preset tunnel speed U_{pre} and the Schiltknecht speed U_{Schilt} taken in the front of the tunnel. TNO corrects the hotwire output V_{HW} for the difference between tunnel speed and Schiltknecht speed:

$$V_{HW\_corrected} = V_{HW} * U_{pre} / U_{Schilt}. \quad (2.1)$$

ECN has been taking measurements with the hotwire probe directly next to a separate Schiltknecht meter inside test section. This has been done at least at the beginning and end of each session and in some occasions also at instances in between. In this way we obtain an additional correction for differences between $V_{HW\_corrected}$ and in situ velocity, *e.g.* due to temperature drift. This correction is applied in the ECN post processing.

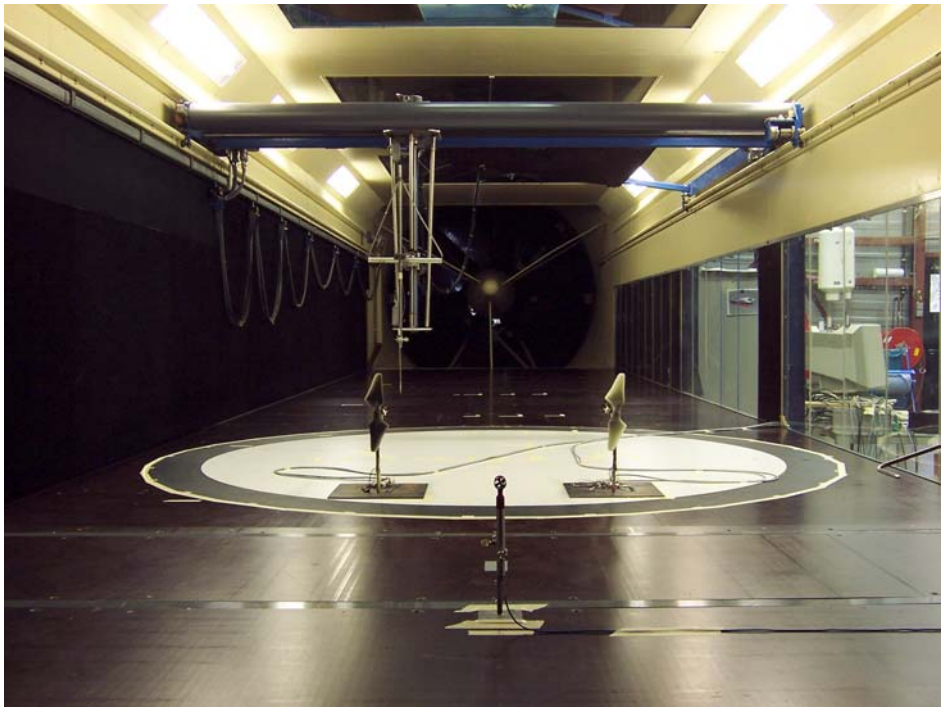

Figure 2.2 *View of the measurement section of the tunnel with the traverse system. In the front center the Schiltknecht anemometer is placed on the floor. In the back of the tunnel the fan can be seen.*

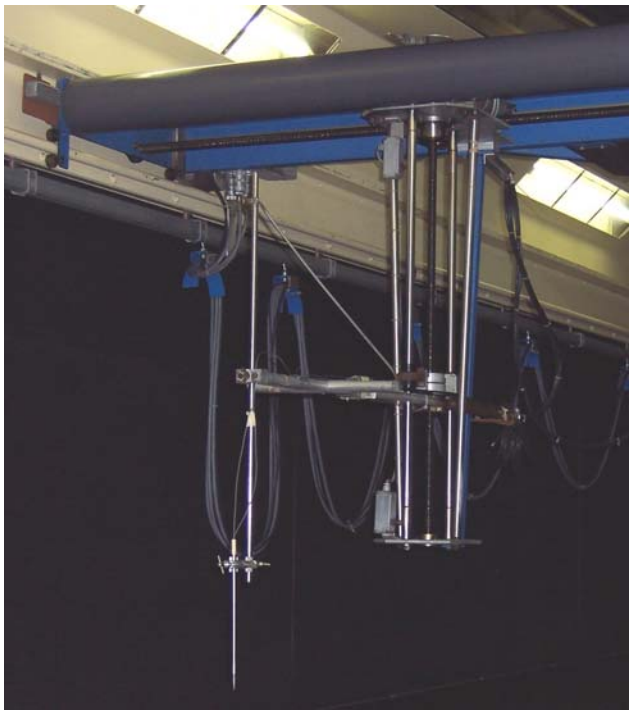

Figure 2.3 *Close up of the hotwire traverse system and probe suspension.*

3. DATA QUALITY AND PREPROCESSING

3.1 Sampling, Filtering and Averaging

The hotwire data are collected and preprocessed via the TNO equipment. At each location series of 20 seconds of instantaneous velocity u in along-tunnel direction x and velocity w in vertical direction z were taken and filtered by a low pass filter with filter frequency of half the sampling frequency. The sampling frequency during the ECN measurements of May 2003 was 200 Hz and 500 Hz during the November 2003 measurements. Tests by ECN have shown that the hotwire results do not change significantly when the sampling frequency is varied within this range. The time mean velocities in x and z direction are denoted as U and W, respectively. Velocity variations $u'=u-U$, $w'=w-W$ are retained to determine the turbulent Reynolds stress $\langle u'w' \rangle$ ($\langle \ldots \rangle$ denotes time averaging). Standard deviations σ_u, σ_w of both u and w time series are converted into turbulence intensities according to

$$I_x = \frac{\sigma_u}{\sqrt{U^2 + W^2}}, \quad I_z = \frac{\sigma_w}{\sqrt{U^2 + W^2}}. \tag{3.1}$$

In total ECN carried out 6 hotwire scan sessions in an empty tunnel. Table 3.1 lists the sessions and gives a general description. Sessions 008, 014 and 031 contain vertical profiles whereas 009 and 016 contains profiles in the across-tunnel (y) direction and 033 yields a profile in the along-tunnel direction at one vertical level. To scale velocity data an appropriate choice for the speed is needed. Since the actual mean speed differs from the nominal speed set by the tunnel operator, we here use the hotwire-measured U velocity at the foremost location at y=0, z=267 mm as the representative tunnel velocity U_t (see table 3.1).

Table 3.1 *Overview of empty tunnel sessions during entries 1 and 2 (May and November 2003), U_t is representative tunnel velocity used for scaling.*

Session	*Date*	*Description*	U_t
ecn008	16:15, May 21, 2003	z-profiles along centerline	6.14
ecn009	09:23, May 22, 2003	horizontal y-profiles at x=0 and 2500 mm	6.26
ecn014	14:26, June 03, 2003	z-profiles along centerline	8.27
ecn016	09:08, Nov 20, 2003	horizontal y-profiles at x=0 and 4000 mm	8.23
ecn031	12:50, Nov. 27, 2003	z-profiles along centerline	9.00
ecn033	15:54, Nov. 27, 2003	horizontal x-profile at centerline	8.28

3.2 Angle Between Tunnel Flow and Horizontal

In all data sets a nonzero angle (α) between flow direction and the horizontal of about 2 to 4 degrees is reported. In general the absolute angle increases with increasing distance form the tunnel floor, but even very close to the floor it has a finite value of about 2 to 3 degrees. In Appendix A the angle at floor level (z=0) has been approximated by vertical extrapolation. Since it is expected that vertical velocities are zero at the floor, the angle of the flow contains a bias of at least this extrapolated value, or 'correction angle'.

The correction angles are listed in tables A.1 and A.2 in Appendix. Appendix A discusses the analysis of the angle (α) the correction angles for all sessions in more detail. It is concluded that the correction angle does not show any systematic structure in the along-tunnel direction, however it does change over the width of the tunnel.

We presume the angle is partly caused by errors in the probe positioning that cause partial projection of the horizontal velocity on the vertical. Besides, the barrier placed in the up-stream part of the channel to set up the boundary layer profile may induce vertical velocities. Finally, a rotation of the flow in the cross-sectional plane of the tunnel may be present. Appendix A discusses this in more detail. Since for each data set different angles are found, the cause of the flow angle cannot be clearly identified yet. From appendix A it is at least clear that the correction angle is independent of the wind speed.

To conclude, the correction angles from the analysis in Appendix A are considered as conservative values. U and W data discussed in this report have all been corrected correspondingly. Turbulent quantities have not been corrected for the angle error.

4. VELOCITY PROFILES

4.1 Vertical Profiles in the Tunnel Center

During the first two entries (May and November 2003) vertical profiles of the horizontal velocity along the center line of the tunnel have been established. Figures 4.1-4.3 show the profiles at various x-locations for session 008, 014, and 031, taken at tunnel speeds U_t of 6.14, 8.27 and 9.0 m/s, respectively. For each location a fit has been made to the log-shape profile representative for neutral boundary layer flows with constant shear stress in the vertical:

$$U(z) = \frac{u_*}{\kappa} \ln\left(\frac{z}{z_0}\right) \tag{4.1}$$

with u_* the friction velocity, κ=0.4 the Von Kármán constant and z_0 the roughness length.

Tables 4.1 and 4.2 list the friction velocity and roughness length derived form the fits.

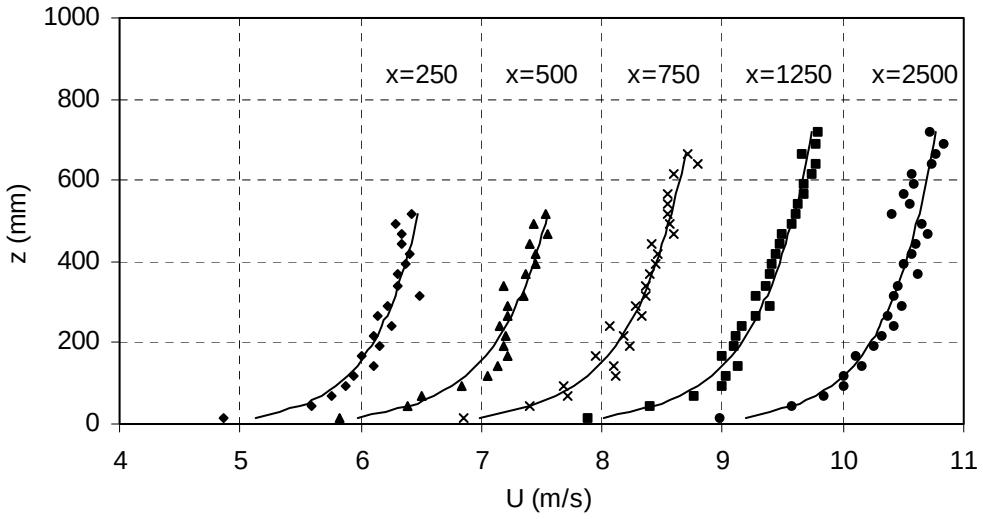

Figure 4.1 *Vertical profile of horizontal velocity U at 5 x-locations (x in mm) along the centerline (y=0) of the tunnel. U_t =6.14 m/s. Drawn lines are fits to the log profile for neutral constant stress boundary layers (see eq. 4.1). Every profile for x>250 has been offset by 1 m/s relative to the preceding profile.*

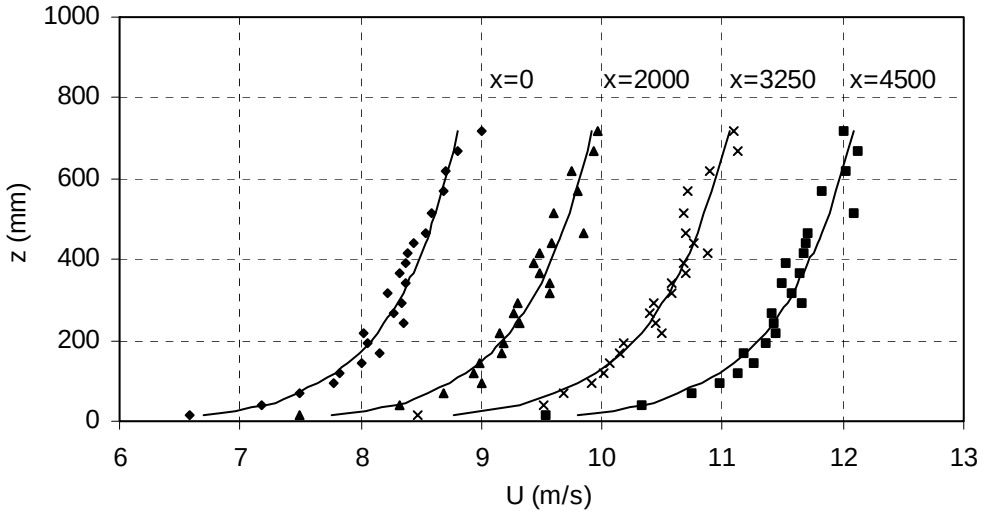

Figure 4.2 *As figure 4.1, but for session 014, U_t =8.27 m/s. Profiles for x>0 have been offset by 1 m/s relative to the preceding profile.*

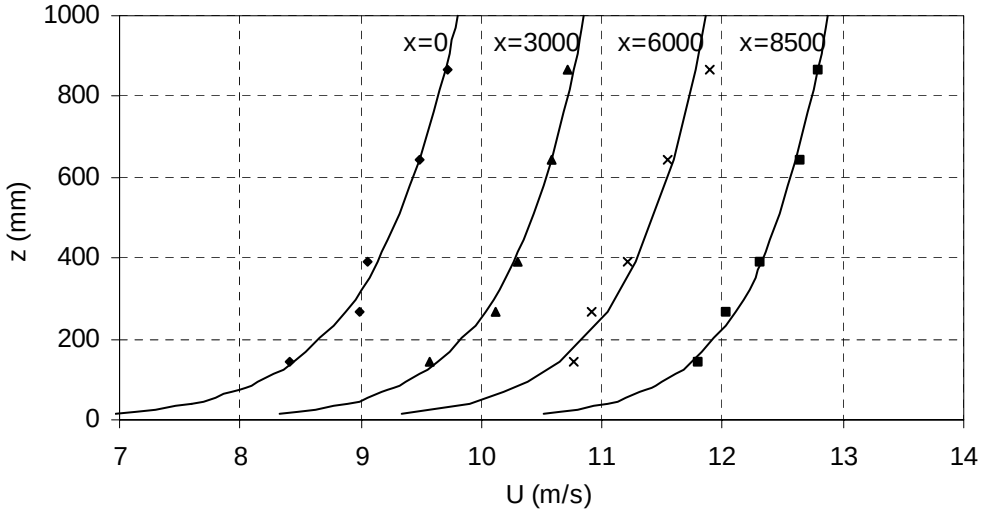

Figure 4.3 *As figure 4.1, but for session 031, U_t =9.0 m/s. Profiles for x>0 have been offset by 1 m/s relative to the preceding profile.*

Tables 4.1 and 4.2 respectively list the friction velocity u_* and roughness length z_0 as derived from the least-squares fits with the log profile of equation (4.1) for each x. The fits include all data in each profile.

Table 4.1 *Friction velocity u_* and the session mean, $\bar{u}_*$, (m/s) from the fits of the vertical profiles of session 008, 014, and 031 to the log profile of equation (4.1).*

Position (x, mm)	*Friction velocity u_* (m/s)*		
	ecn008 U_t*=6.14 m/s*	*ecn014* U_t*=8.27 m/s*	*ecn031* U_t*=9.00 m/s*
0		0.23	0.28
250	0.16		
500	0.18		
750	0.19		
1250	0.19		
2000		0.23	
2500	0.17		
3000			0.25
3250		0.24	
4500		0.24	
6000			0.25
8500			0.23
Mean, $\bar{u}_*$	0.178±0.01	0.24±0.006	0.25±0.02
$\bar{u}_*/U_t$	0.029±0.002	0.029±0.001	0.028±0.002

Table 4.2 *Roughness length z_0 (mm) derived from the fits of the vertical profiles of session 008, 014, and 031 to the log profile of equation (4.1).*

Position (x, mm)	*Roughness length z_0 (mm)*		
	ecn008 U_t*=6.14 m/s*	*ecn014* U_t*=8.27 m/s*	*ecn031* U_t*=9.00 m/s*
0		$1.2*10^{-4}$	$7.2*10^{-4}$
250	$3.9*10^{-5}$		
500	$3.5*10^{-4}$		
750	$4.0*10^{-4}$		
1250	$3.6*10^{-4}$		
2000		$1.4*10^{-4}$	
2500	$7.7*10^{-5}$		
3000			$1.2*10^{-4}$
3250		$2.6*10^{-4}$	
4500		$2.5*10^{-4}$	
6000			$1.3*10^{-4}$
8500			$3.5*10^{-4}$
Mean	$(2.3\pm1.7)*10^{-4}$	$(1.9\pm0.7)*10^{-4}$	$(3.3\pm2.8)*10^{-4}$

The data of the three sessions in general fit the log profiles quite well. The shape is well conserved along the tunnel. It can be seen, nonetheless, that at most x-positions in figures 4.1 and 4.2 the fit deviates from the data in about the lower 150 to 200 mm of the profiles. Here the fits tend to underestimate the measured velocity shear: separate fits to the lower 167 mm yields u_* values that are about 25% larger than the values in table 4.1. The scatter around the fits makes it hard to further distinguish systematic deviations from the log profile, though.

The bottom row of table 4.1 shows that u_* scales well with the tunnel velocity. Analysis of the along-tunnel trend in scaled u_* in Appendix B suggests a slight decrease of about 9% over 10 meter. The consistency of the quality of the fits along x and the enhanced in shear in the lower 150 mm are also found in (TNO 1995).

Analysis of the turbulent vertical shear stress (Reynolds stress $<u'w'>$) in Appendix B indicates that in the front of the test section the stress does not vary significantly with height. This property is retained at least in the first 3 meters of the test section. It cannot be stated with certainty if the Reynolds stress further down the tunnel is vertically dependent or not. For the first meters of the test section, at least, it further indicates that the vertical velocity profiles represent a neutral atmospheric boundary layer quite well. The vertically averaged Reynolds stresses decrease more strongly with distance along the tunnel than u_*: about 50% over 8.5 m.

We conclude that the averaged vertical velocity profiles in the tunnel are representative for neutral conditions up to a height of at least 80 cm in the tunnel, or 320 m in practice, assuming a scale 1:400. In general the profiles show an increase in speed with increasing distance to the inlet, but the shape of the profiles is well conserved, as indicted by the fact that u_* does not vary significantly with x. Also, u_* scales well with the tunnel velocity U_t. The roughness length values ranges from $0.4*10^{-4}$ to $7.2*10^{-4}$ mm this is the right order of magnitude to represent offshore conditions with calm sea (Garratt, 1992) (i.e., 0.016 to 0.29 mm, assuming a scale factor of 400) but shows no systematic dependence on either x or tunnel velocity.

4.2 Horizontal Velocity Profiles

4.2.1 Profiles in *y*

Figure 4.4 shows the scaled cross-sectional velocity profiles from session 009 at x=0 at three heights in the tunnel. The scatter is in the order of 3% of the average velocity. Apart from the decrease towards the side walls, a systematic increase of at most 3% from left to right over the tunnel width is found. Also, the shape of the vertical profiles is seen to vary considerably from y position to y position.

Figure 4.5 shows the profile at z=267 for two tunnel speeds and various x. Here it can be seen that the velocity increases in x for all y. This will be further discussed in the next section. Again, an increase from left to right is found, also for large x.

From both plots it is clear that towards the side walls velocity decreases (although occasional increases are found). The velocity maximum is found to the right of the center. It is unclear what causes this asymmetry. The scatter in the data is too large and the number of vertical levels is too limited to make more detailed statements about the quality of the vertical profiles across the tunnel.

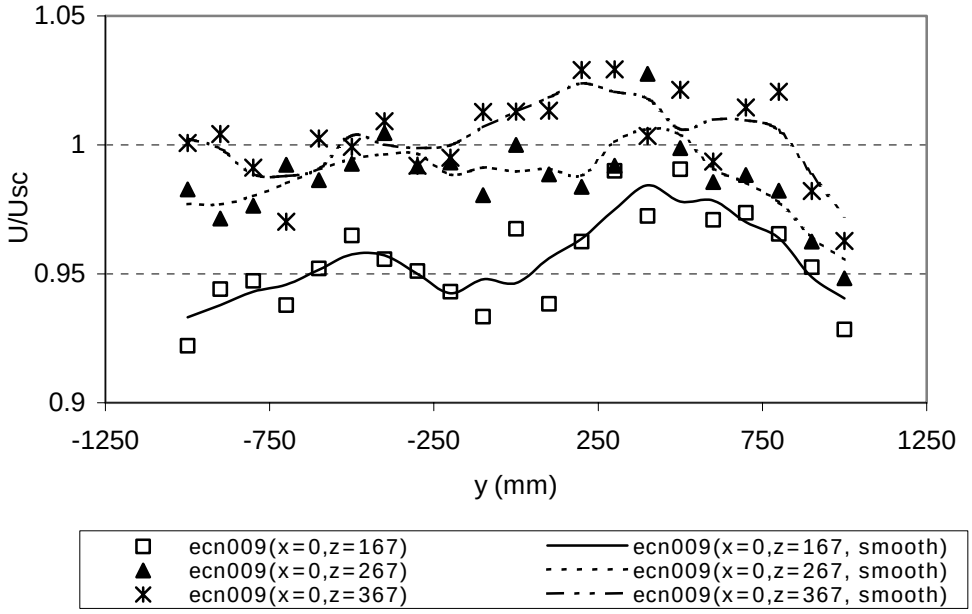

Figure 4.4 *Across-tunnel velocity profile at different heights for session 009. Velocities are scaled by U_t = 6.26 m/s. Markers indicate actual data, lines pass through 3-point smoothed values.*

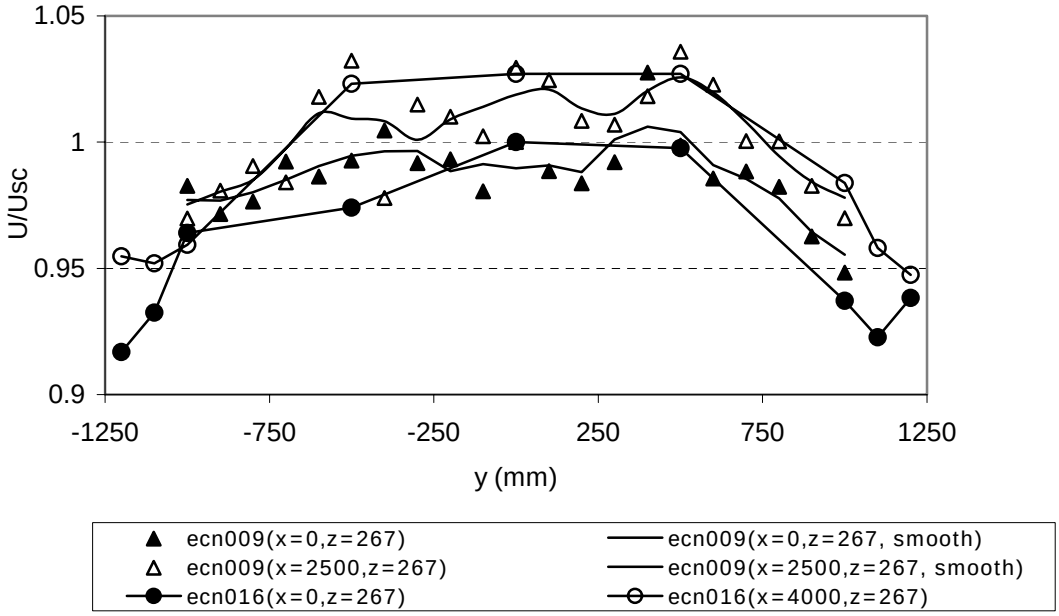

Figure 4.5 *Across-tunnel velocity profiles for different x-positions at hub height (267 mm) for sessions 009 and 016. The velocities are scaled by U_t = 6.26 and 8.23 m/s respectively.*

4.2.2 Profiles in *x*

As already indicated in section 4.1 the *U* velocities in lower half of the tunnel increase in flow direction along the tunnel axis. In figures 4.1 to 4.3 the increase is clearly visible above about 100 mm from the floor. Figure 4.6 shows the variation in flow direction of *U* at *z*=267 mm for sessions 008, 014, 031and 033. From this it is clear that the lower U_t, the higher the relative increase. Table 4.3 shows the values of relative increase over 10 meter along the tunnel.

Table 4.3 *Estimate of the scaled along-tunnel increase of horizontal velocity over 10 meter from linear least squares fits.*

	ecn008	*ecn014*	*ecn033*	*ecn031*
Tunnel velocity U_t (m/s)	6.14	8.27	8.28	9.00
Mean $(\partial U/\partial x)/U_t$ over 10 m (%)	11±7	8±3	6±2	2±1

The increase in speed is explained as follows: In the front of the test section the velocity profile above the tunnel floor represents a scaled atmospheric boundary layer. In such a boundary layer the shear is independent of altitude. However, in an infinitely long four-sided rectangular channel the shear linearly decreases with distance to the wall, approaching zero towards the tunnel center. The velocity profile in the tunnel will gradually adapt from the atmospheric situation to the rectangular channel situation when travelling in flow direction. Since the shear at greater altitudes will decrease, while the pressure gradient is acting equally at all altitudes, the velocity at higher altitude will increase during this adaptation.

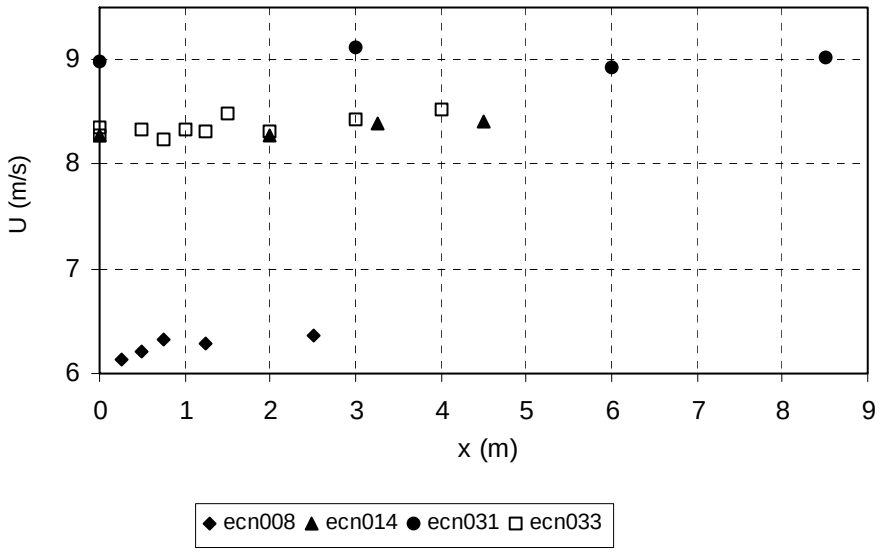

Figure 4.6 *Horizontal velocity U (m/s) along the tunnel axis at z=267 mm for 4 sessions. If no data were available at z=267 mm, values have been estimated by interpolation.*

A conservative estimate of the pressure gradient can be derived from the speed up in flow direction at z=489 mm. To estimate the along-tunnel pressure gradient, we assume stationary condition and neglect shear effects. The pressure gradient can then be estimated from the momentum equation:

$$\frac{\partial p}{\partial x} = -\frac{1}{2}\rho\frac{\partial U^2}{\partial x}, \tag{4.2}$$

where U the velocity at z=489 mm.

Figure 4.7 shows $\frac{1}{2}U^2$ as function of along-tunnel position for three sessions for which U at 489 mm could be determined.

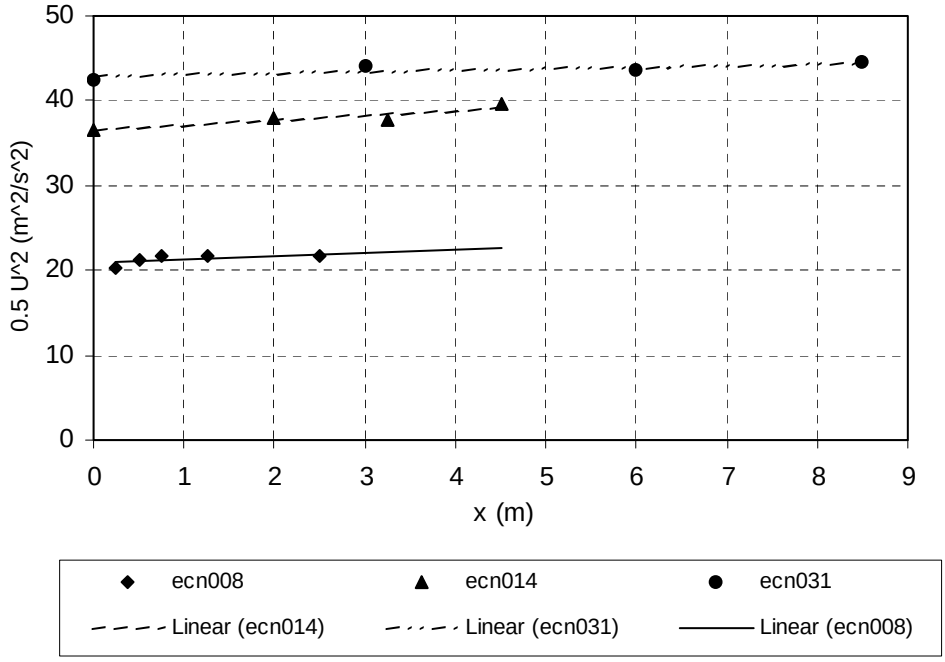

Figure 4.7 *Along-tunnel profile of $\frac{1}{2}U^2$ at z=489 mm, lines are least squares linear fits.*

The mean horizontal gradient in $\frac{1}{2}U^2$ follows from linear least squares fitting. The slopes are displayed in table 4.4 below.

Table 4.4 *Estimate of the along-tunnel pressure gradient from mean horizontal gradient in $\frac{1}{2}U^2$ and the estimated frictional drag of the tunnel.*

(ρ =1.3 kg/m^3)	*ecn008*	*ecn014*	*ecn031*
Tunnel velocity U_t (m/s)	6.14	8.27	9.00
Mean dynamic pressure gradient $\frac{1}{2}\partial U^2/\partial x$ (Pa/m)	0.46	0.74	0.25

From the mean gradients in $\frac{1}{2}U^2$ in table 4.4 the mean dynamic pressure gradient is estimated to be 0.5 ± 0.3 Pa/m.

5. CONCLUSIONS

The boundary layer velocity profiles in the TNO-tunnel turn out to be a good representation of neutrally stable offshore atmospheric conditions scaled by a factor of 400. The profiles follow the logarithmic shape up to a height of at least 800 mm, *i.e.* 320 meters in reality. The roughness length derived from fitting log-shape profiles is about ranges from $0.4*10^{-4}$ to $7.2*10^{-4}$ mm, *i.e.* 0.02 to 0.3 mm in reality. This is the right magnitude for calm-sea conditions (Garratt, 1992). Table 5.1 summarizes the most important results.

Table 5.1 *Most important results from the analysis of the empty boundary layer tunnel.*

Characteristic	*neutrally stable, offshore atmosphere in reality*	*empty TNO-tunnel (6-9 m/s)*
Vertical velocity profile	logarithmic	logarithmic up to 80 cm height (320 m on scale) over first 9 m (3600 m on scale); separate fits of lower 17 cm yield 25% larger values for u_*;
Horizontal velocity profile	flat	Varies by 3% over tunnel width between 17 and 37 cm height (68m - 148m on scale).
Friction velocity u_*	constant	Varies by 9% over first 9 meters.
Shear stress (Reynolds stress, $<u'w'>$)	'independent' of height	'Independent' of height in first 4.5 meters; decreases about 30% in 80 cm height in next 4.5 meters.
Surface roughness z_0	0.2 mm	$0.4\text{-}7.2*10^{-4}$ mm (0.02-0.3 mm on scale)
Dynamic pressure gradient in wind direction	'none'	≈ -0.5 Pa/m (-1.3 Pa/km on scale)
Angle between flow and horizontal, $\|\alpha\|$	'none'	2° to 7°
Correction angle ($\|\alpha\|$ at z=0, degrees)	0°	2° to 3°

The horizontal velocity in the lower half of the tunnel increases over de tunnel length because of a gradual transition of the vertical velocity profile from the intended constant shear profile to a profile with linearly decreasing shear. From the acceleration, the pressure gradient in flow direction is assessed to be in the order of 0.5 Pa/m. This pressure gradient is not present in the outside atmosphere.

The friction velocity decreases along the length of the tunnel by about 9% over 10 meter. This relatively slight decrease reflects the observation that the adjustment from a constant-stress to linear-stress boundary layer is too gradual to significantly degrade the profiles. In the first 4.5 meters the Reynolds shear stress does not significantly depend on height. At 6 and 8.5 meters distance the shear stress decreases by about 30% in the first 80 cm height. The horizontal velocity measured between 167 and 367 mm above the floor increases by at most about 3% from left to right across the tunnel (looking into the flow direction), apart of the expected decrease towards the sidewalls. The velocity maximum is located to the right of the tunnel axis, looking into flow direction.

The data show an angle α between the flow and the horizontal of a few degrees, even very close to the floor. This would imply an unrealistically large vertical velocity component. We suggest the angle is at least partly due to erroneous probe orientation. A correction angle has been derived by vertical extrapolation and has been applied to all U and W data.

6. REFERENCES

Corten, G.P.(2001): *Flow Separation on Wind Turbine Blades*, PhD Thesis Utrecht University, January 2001.

Corten, G.P. and P. Schaak, (2003): *Increase of Wind Farm Production by Reduction of the Axial Induction: Heat and Flux* , ECN-RX--03-061, EWEC 2003, Madrid, Spain.

Corten, G.P. and P. Schaak (2004): *More Power and Less Loads in Wind Farms: 'Heat and Flux'*, EWEC, London, UK, 2004.

Corten, G.P., Lindenburg, K., Schaak, P. (2002) *Method and Assembly Relating to Energy from Flows, such as a Wind Farm*, patent application, July 15, 2002.

Garratt, J.R. (1992): The Atmospheric Boundary Layer, Cambridge Univ. Press. 1992, 316 pp.

Monseur, A. (2004): *Wind Tunnel Quality for Heat and Flux Experiments*, Internship report, ECN Sept. 2003-Jan. 2004

TNO (1995), Karakterisering tunnel 4, TNO Code 0V-150B-0H-0R, TNO Apeldoorn, February 28,1995.

Appendix A: Angle α Between Flow and Horizontal

Vertical velocities measured during the tunnel entries differ significantly form zero, even close to the floor. Typically, *W* values are of the order of 5 to 10% of the *U* values. In other words, the hotwire probe reports a deviation of the flow from the horizontal with angle α=arctan(*U,W*) of about 2 to 6 degrees. Because of symmetry in the configuration this is unexpected. Moreover, this is not observed in the real atmosphere. In this appendix a more detailed analysis of the angle is given. This yields a correction angle that has been applied to all U and W data in this report.

• Profiles of α in *z*

In general α increases with increasing distance form the floor. Figure A.1 illustrates the variation of α in *z*.

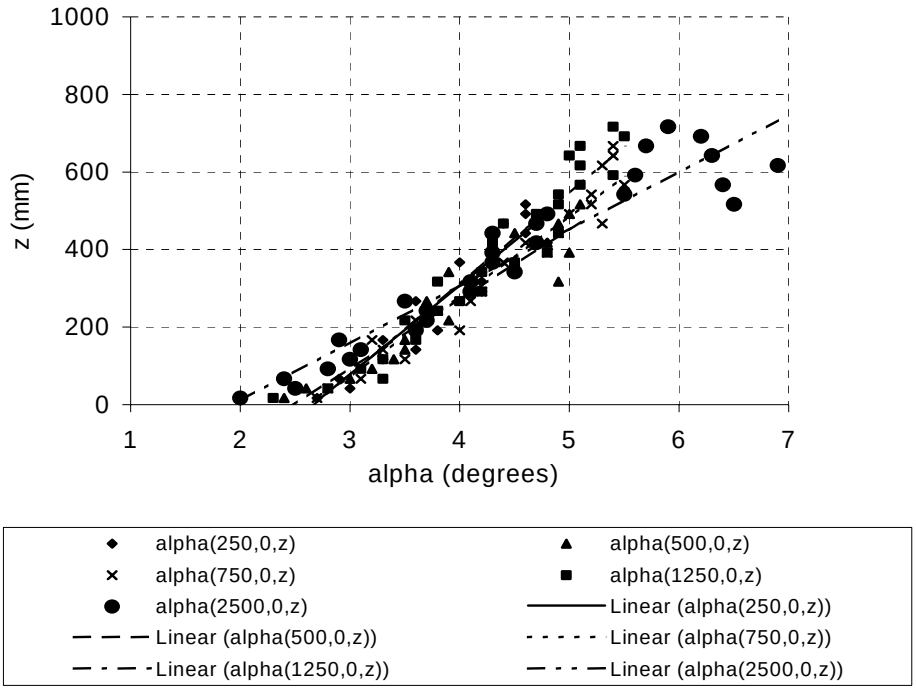

Figure A.1 *Angle α (degrees) between air flow and horizontal as reported by the hotwires as function of position along the axis of the tunnel for session 008 (U_t=6.14 m/s). Drawn lines are linear least-squares fits. The offsets of the fits are listed in table A.1.*

Both the slope and offset (see also table A.1) of the fits for session 008 in figure A.1 vary quite randomly in *x*. The same can be concluded for sessions 014 and 031 (figures A.2, A.3) with higher tunnel velocity. Although the latter profiles show higher mean values, no clear correlation could be found between tunnel velocity and mean angle. For sessions 016, 031 and 033 negative angles have been reported. Since the hotwire probe cannot distinguish the sign of a velocity component, we do not know whether the reported angles have reliable sign. What we do know is that vertical velocities should vanish at the tunnel floor. This has been used when correcting the data for errors in the angle of the flow (see below). For the sake of comparison the negative of the angles is shown in plots of sessions 016, 031, and 033.

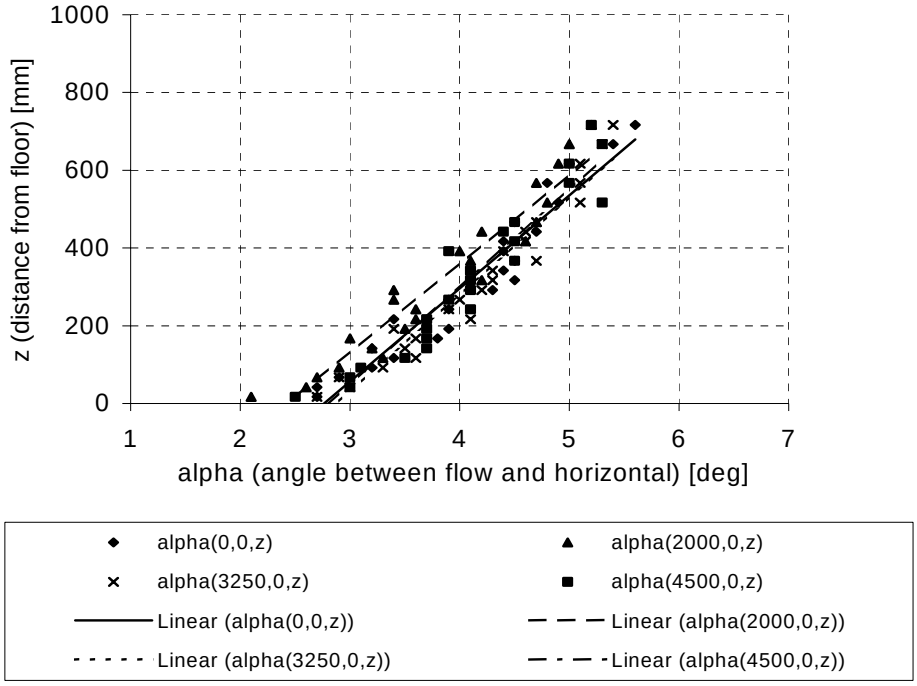

Figure A.2 *As figure A.1, but for session 014 (U_t=8.27 m/s).*

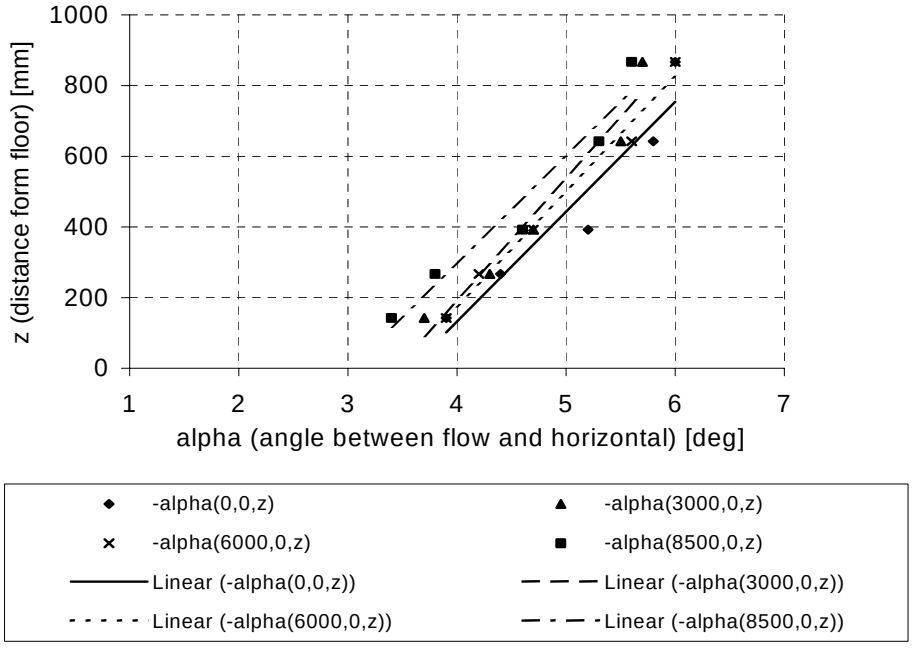

Figure A.3 *As figures A.1 and A.2, but for session 031 (U_t=9.0 m/s) Here the negative of the reported angle has been plotted.*

Table A.1 lists the correction angles that follow form the vertical fits shown above. These correction angles have been applied to all *U* and *W* data presented in this report. The *W*

component has been corrected such that its value approaches zero towards the floor. In this way, the uncertainties in the sign of both *W* and angle cancel.

Table A.1 *Correction angle (degrees) for each session and for each x location determined from linear extrapolation of vertical profiles of angle α. For session 033 no vertical profiles are available, hence a conservative limit of the correction angle has been estimated form comparable sessions (min(|α_{033}|)=3.1°>2.5°).*

	Correction angle			
x (mm)	*ecn008*	*ecn014*	*ecn031*	*ecn033*
0		2.7°	-3.6°	-2.5° for all *x*
250	2.7°			
500	2.5°			
750	2.7°			
1250	2.7°			
2000		2.4°		
2500	1.9°			
3000			-3.4°	
3250		2.9°		
4500		2.8°		
6000			-3.4°	
8500			-3.0°	

Table A.2 *Correction angle (degrees) for y-profile sessions. For session 009 the correction has been determined from linear extrapolation of moving averages of the angles at the three vertical positions z=167, 267, 367 mm. For session 016 a minimum angle has been estimated since no vertical profiles are available (min($|\alpha_{016}|$)=2.9°).*

	Correction angle	
y (mm)	*ecn009*	*ecn016*
-1000	2.2°	
-900	1.9°	
-800	1,8°	
-700	1.9°	
-600	2.0°	
-500	1.7°	
-400	2.5°	
-300	2.5°	
-200	2.6°	
-100	2.6°	
0	2.8°	-2.5° for all y and both x
100	2.9°	
200	2.8°	
300	3.1°	
400	3.4°	
500	3.6°	
600	3.6°	
700	3.1°	
800	2.8°	
900	2.4°	
1000	2.4°	

- Profiles of α and Correction Angle in *y*

Although systematic dependency of α on *x* could not be established, the variation of α in *y* does show a recurring structure. It is similar to the variation of *U* in *y* (section 4.2): for all *x,* α has a local maximum, generally right of the center and local minima between *y*=±750 and ±1250. The absolute angle has a general tendency to increase from left to right across the tunnel, see figure A.4. Also in this figure it can be seen that on average α increases with increasing height but that scatter, even in the 3-point averaged data is still considerable.

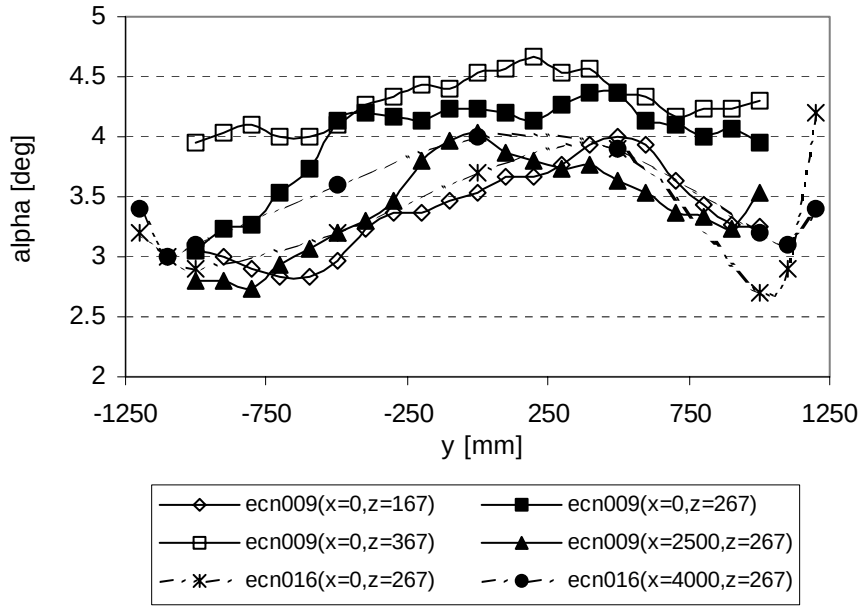

Figure A.4 *Across-tunnel profile of angle α (degrees) for various x-positions and heights for two sessions. Data of session 009 have been averaged laterally by a 3-point moving average (2-point for the outer points). Negative of reported angles are shown for session 016. U_t = 6.26 m/s for session 009, U_t = 8.23 m/s for session 016.*

The variation in *y* is also reflected in the correction angle. As can be seen in figure A.5 an increase from left to right and decrease towards the side walls is retrieved after vertical extrapolation.

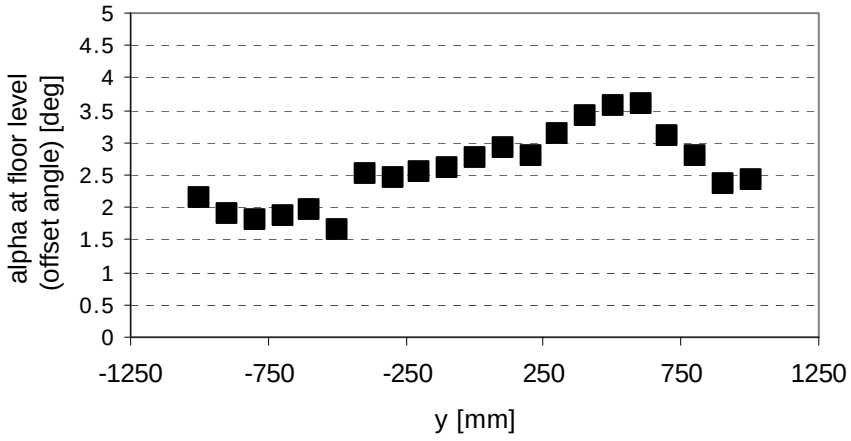

Figure A.5 *Across-tunnel profile of angle α (degrees) at floor level (i.e., correction angle) for x=0 of session 009 (U_t = 6.23 m/s). Angles have been determined from linear extrapolation of lateral 3-point moving averages of the angles at z=167, 267, and 367 mm.*

It has been suggested at earlier stages that a rotation of the flow in the cross section of the tunnel exists. This rotation, if present, would be caused by the sideward inflow of the air at the inlet of the tunnel (see also figure A.5). The explanation is the following (see also figure A.6): Where the flow trajectory makes a right turn inside the inlet (see figure 2.1), the flow will experience a centrifugal force proportional to the square of the flow speed. Since the flow speed close to the inlet walls is lower than average and the flow in the center moves faster than average, the centrifugal force induces a rotation such as displayed by figure A.6. Because of symmetry, the rotation in the upper half of the tunnel should be the reverse of that in the lower half. The general tendency of the angle to increase across the tunnel from left to right (see figure A.4) is consistent with this rotation pattern. It should be noted that the sign of the angles is uncertain, so at this stage we cannot be conclusive about the rotation patterns of figure A.6. More extensive scans over the entire vertical are needed to substantiate further statements about cross-sectional rotation.

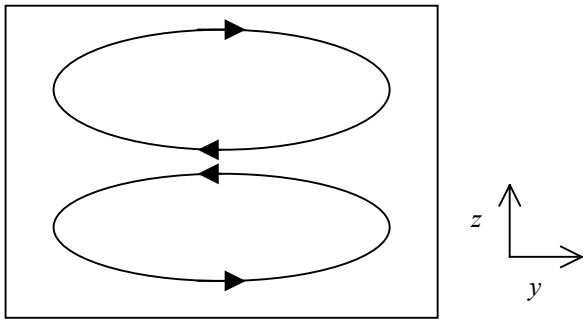

Figure A.6 *Sketch of rotation that would be present in the cross-sectional plane of the tunnel due to curvature of the tunnel inlet.*

Appendix B: Reynolds Stress <u'w'>

To further support our statements on the quality of the boundary layer profiles in the lower 800 mm a more detailed analysis of the Reynolds stress <u'w'> is made in this appendix.

- Profiles of Reynolds Stress in *z*

Figures B.1 through B.3 show profiles of the Reynolds stresses <u'w'> as function of position and tunnel speed for sessions 008, 014, and 031. These stresses are determined directly from the hotwire output time series as described in section 3.1 and are not corrected for angle errors.

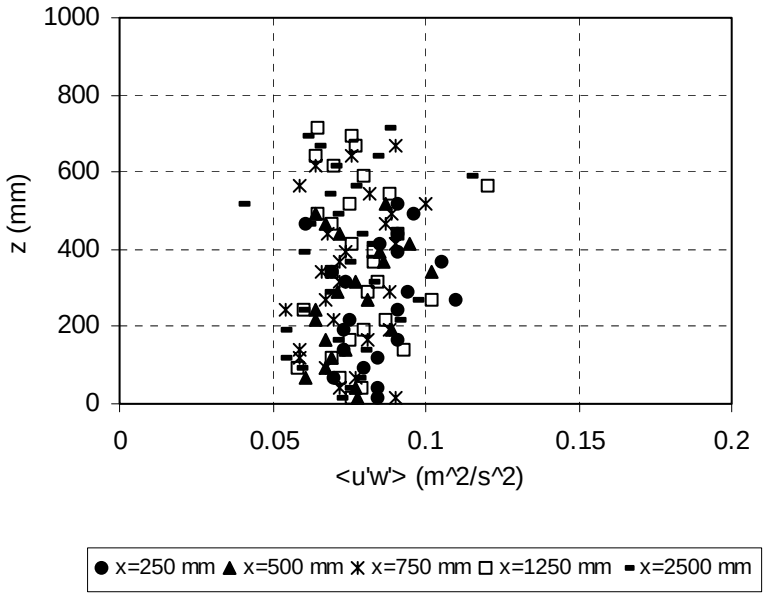

Figure B.1 *Reynolds stress <u'w'> (m^2/s^2) for session 008 (U_t=6.14 m/s) at five x-positions.*

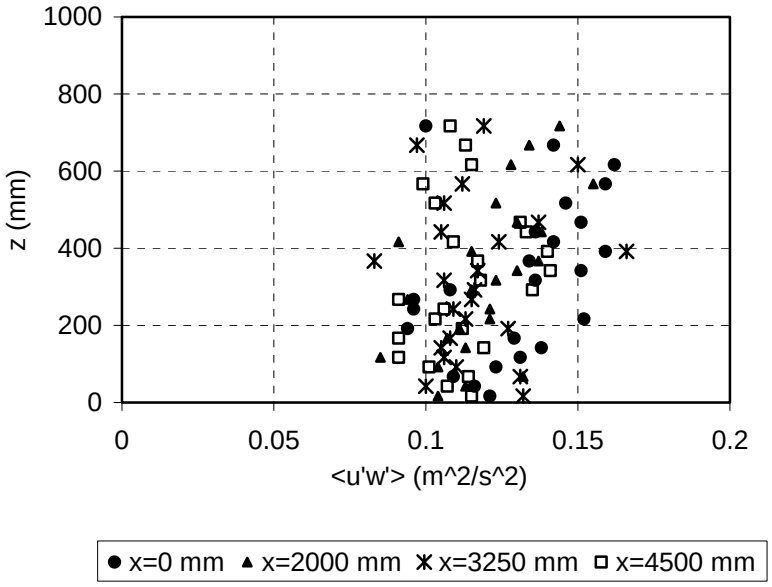

Figure B.2 *As figure B.1 but for session 014, U_t=8.27 m/s.*

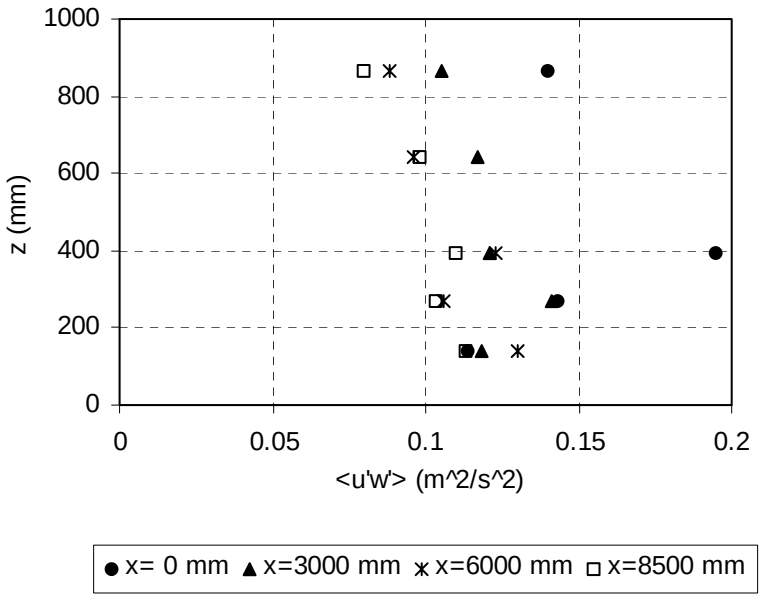

Figure B.3 *As figures B.2 and B.3 but for session 031, U_t=9.0 m/s. Here the negative of the reported stress is shown for comparison with the previous plots.*

Further analysis of the data in figures B.1-B.2 shows that the Reynolds stresses of session 008 and 014 do not depend significantly on height. As for the vertical velocities and angles, the Reynolds stresses for the November 2003 sessions (fig. B.3) have negative sign. Slopes fitted to data in figure B.3 (session 031) deviate from zero beyond the fit error for all profiles except for

x=0. In these three profiles the fits to absolute stress suggest a decreases with height. It is hard to be conclusive at this stage, however, because the uncertainly in the fit coefficient is large. The averages of the Reynolds stresses for all three sessions are given in table B.1.

Table B.1 *Mean Reynolds stresses for the three sessions for which vertical profiles have been investigated.*

	ecn008	*ecn014*	*ecn031*
Tunnel velocity U_t (m/s)	6.14	8.27	9.00
Mean $<u'w'>$ (m^2/s^2)	0.077±0.013	0.12±0.02	0.12±0.03

The Reynolds stresses and the friction velocity are related by

$$u_*^2 = \sqrt{<u'w'>^2 + <v'w'>^2} \tag{4.2}$$

Since $<v'w'>$ is expected to be smaller than $<u'w'>$ term, at least away from the side walls, u_*^2 should be about at least the value of $<u'w'>$. However, by combining the data of tables 4.1 and table B.1 we find that the mean u_*^2 is about half the mean $<u'w'>$. The difference may be caused by fluctuations in tunnel flow speed due to turbulence in the outside atmosphere. This low-frequency turbulence is not representative for a truly scaled atmospheric boundary layer and leads to an overestimation of the Reynolds stresses.

- Profiles of Reynolds Stress and Friction Velocity in *y*

The vertically averaged Reynolds stresses decrease along the tunnel axis by tens of percents. This can be seen in figure B.4 where the Reynolds stresses scaled by U_t^2 are shown. For comparison, the scaled values of the friction velocities of table 4.1 are plotted in figure B.5. The u_* data show qualitatively similar behavior but have a much weaker decrease. Table B.2 summarizes the relative decrease over 10 meter. It is unclear why the Reynolds stresses decay about 5 times faster than friction velocities. The decay of turbulent stresses is attributed to the dissipation of turbulent kinetic energy along the trajectory form the principal source region (the barrier in the front of the tunnel).

Table B.2 *Relative decrease of Reynolds stress and friction velocity over 10 m along the tunnel axis.*

	$<u'w'>/U_t^2$	u_*/U_t
Relative decrease over 10 m	43±10%	9±6%

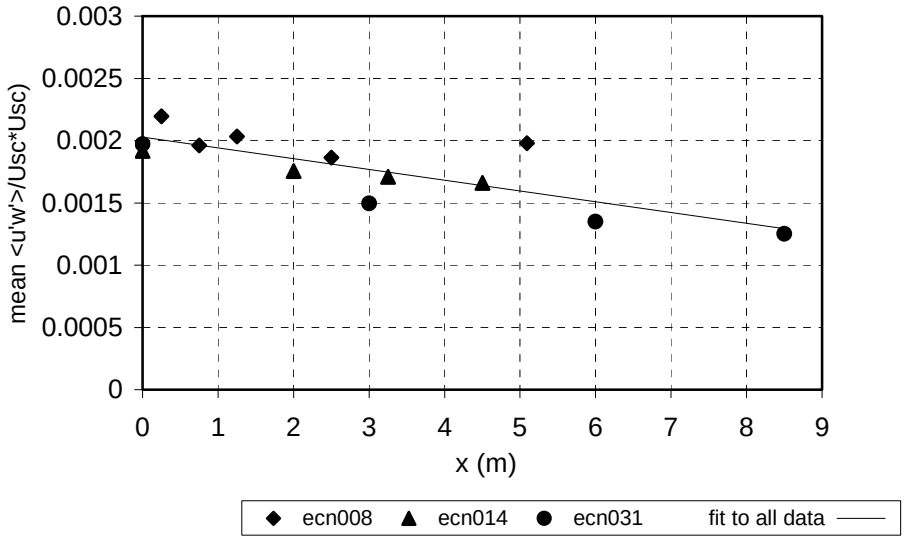

Figure B.4 *Mean Reynolds stress along tunnel axis for three sessions.*

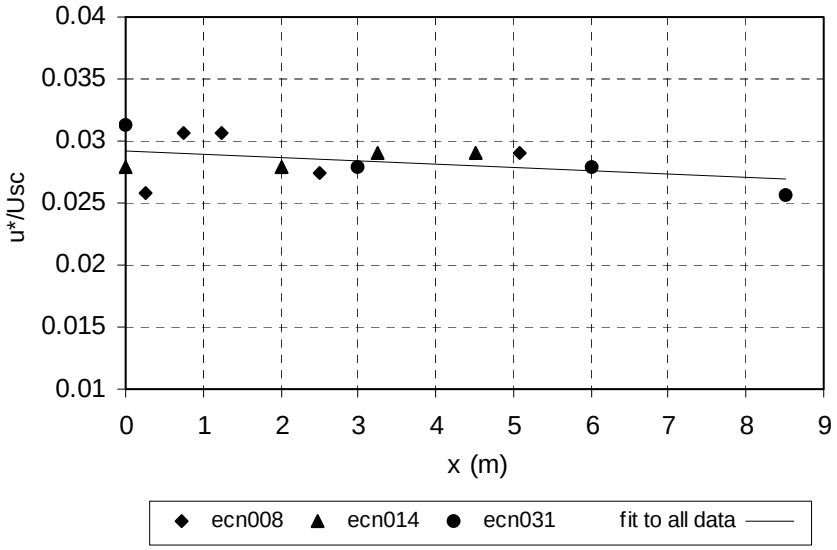

Figure B.5 *Scaled friction velocities from the log-profile fits of sessions 008, 014 and 031.*